Crack fronts and damage in glass at the nanometre scale



2003 J. Phys.: Condens. Matter 15 S2377

(http://iopscience.iop.org/0953-8984/15/31/313)

INSTITUTE OF PHYSICS PUBLISHING JOURNAL OF PHYSICS: CONDENSED MATTER

J. Phys.: Condens. Matter **15** (2003) S2377–S2386 PII: S0953-8984(03)62441-0

# Crack fronts and damage in glass at the nanometre scale

**Christian Marlière[1,3], Silke Prades[2], Fabrice Célarié[1], Davy Dalmas[2], Daniel Bonamy[1,2], Claude Guillot[2] and Elisabeth Bouchaud[2]**

[1] Laboratoire des Verres, UMR CNRS-UM2 5587, Université Montpellier 2, CC 69, Place Bataillon, F-34095 Montpellier Cedex 5, France
[2] Service de Physique et Chimie des Surfaces et Interfaces, DSM/DRECAM/SPCSI, CEA Saclay, F-91191 Gif sur Yvette, France

E-mail: christian.marliere@ldv.univ-montp2.fr

Received 22 April 2003
Published 23 July 2003
Online at stacks.iop.org/JPhysCM/15/S2377

**Abstract**

We have studied the low-speed fracture regime for different glassy materials with variable but controlled length scales of heterogeneity in a carefully controlled surrounding atmosphere. By using optical and atomic force microscopy techniques, we tracked, in real-time, the crack tip propagation at the nanometre scale over a wide velocity range ($10^{-3}$–$10^{-12}$ m s$^{-1}$ and below). The influence of the heterogeneities on this velocity is presented and discussed. Our experiments reveal also—for the first time—that the crack progresses through nucleation, growth and coalescence of nanometric damage cavities within the amorphous phase. This may explain the large fluctuations observed in the crack tip velocities for the smallest values. This behaviour is very similar to that involved, at the micrometric scale, in ductile fracture. The only difference is very probably due to the related length scales (nanometric instead of micrometric). The consequences of such a nano-ductile fracture mode observed at a temperature far below the glass transition temperature, $T_g$, in glass is also discussed.

(Some figures in this article are in colour only in the electronic version)

## 1. Introduction

Despite much work and recent progress, materials fracture still exhibits many puzzling aspects. Two different observations seem particularly difficult to reconcile.

- Brittle materials—the most common example of which is glass—break abruptly, without first deforming, while in ductile materials—such as metallic alloys—fracture is preceded

[3] Author to whom any correspondence should be addressed.

by large plastic deformations. In this latter case, it has been observed [1] that the crack progresses through the coalescence of micrometric damage cavities nucleated from microstructural defects (second phase precipitates, grain boundaries . . .).

- However, quantitative studies reveal that both types of fracture surfaces have a very similar morphology. Fracture surfaces have been shown to be self-affine objects [2, 3] for both brittle and ductile materials. Two self-affine regimes coexist: at small length scales (up to a length $\xi_c$), the roughness exponent $\zeta$ is close to 0.5, whereas at large length scales (from $\xi_c$ to a larger length $\xi$), $\zeta$ is around 0.8. These values of $\zeta$ are *universal*, but $\xi_c$ as well as $\xi$ depends on the kind of material considered, ranging from a few nanometres for glass [4] to a few centimetres for concrete and rocks [5]. It is worth noting that, for ductile materials, $\xi_c$ is of the order of the typical size of the damage cavities when they coalesce [1].

  This strongly suggests that the observed transition between the two self-affine regimes reflects a change from an intra-cavity structure to an inter-cavity one. Such a scenario was first proposed in [1, 6, 7], based on the observation of the roughness of growing cavities before coalescence in an aluminium alloy, and was further developed in a recent paper [8].

The question is how can we reconcile these two observations? A natural supposition is that a ductile-like—up to now undetected—fracture process exists in brittle materials like glass. In this case, the size of the associated damage cavities at coalescence is expected to be equal to the crossover length $\xi_c$, i.e. of the order of ten nanometres. The need for an experimental observation of such an effect was what led to the experiment described in the following. Our new experimental set-up, based on atomic force microscopy (AFM), is described in section 2. Huge velocity fluctuations in the progression of the tip were detected (section 3) and explained by the observation of nanometric cavities developing ahead of the crack tip (section 4). These cavities were proved to be *damage* cavities by using two independent methods (section 5). Finally, the possible origins of these cavities are conjectured and the consequences of such a ductile fracture mode in glass are discussed (section 6).

## 2. Experimental set-up

The design of our experiments should meet the following requirements to achieve the goal described above:

(i) The apparatus should have a very high spatial resolution (a few tenths of nanometres) and work in real-space and real-time (no post-mortem studies). Moreover, it should deal with electrically non-conductive materials. Surface treatments—which limit the spatial resolution (by metal deposition for instance)—are also prohibited. The AFM technology appears then to be the ideal tool that meets all these requirements. Due to the nanometric resolution of AFM we measure crack speeds lower than $10^{-12}$ m s$^{-1}$ with a reasonable acquisition time (15 min between each acquired image).

(ii) The main drawback of AFM resides in its recording time, that cannot be set lower than a few minutes without significant loss in the spatial resolution. It forces us to work in the so-called 'stress corrosion' or 'sub-critical growth' regime [9–11]. The crack behaviour is then controlled by the chemically activated processes with the surrounding environment. A rigorous control of atmosphere and temperature is then necessary.

(iii) The crack progression should be stable and well monitored. This led us to design a mechanical DCDC (double cleavage drilled compression) system [12].

The experimental set-up is illustrated in figure 1. All the experiments are performed at a constant temperature of $22.0 \pm 0.5$ °C in a leak-proof chamber under an atmosphere composed

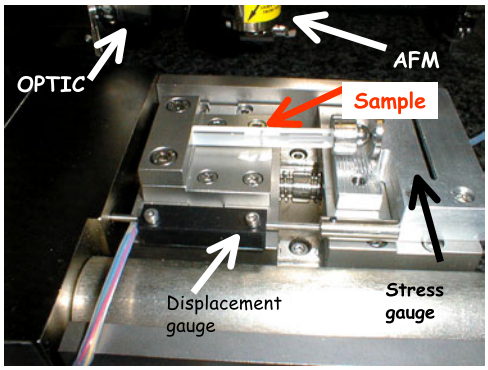


**Figure 1.** Experimental set-up.

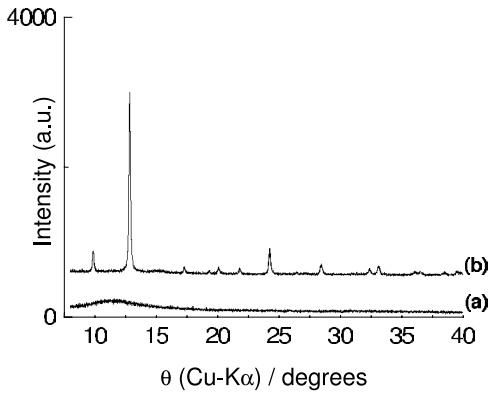


**Figure 2.** X-ray diffraction patterns on lithium alumino-silicate glass-ceramics: (a) sample A in a pure glassy state; (b) sample B in a slightly unglassy state.

of pure nitrogen and water vapour at a relative humidity level of $42 \pm 1\%$ after preliminary out-gassing.

Lithium alumino-silicate glass-ceramics were studied. The main advantage of this kind of material is that its structure can be controlled through an applied thermal treatment [13]. Two types of structures are investigated below. The first one (sample A) corresponds to a pure glassy state as identified by x-ray diffraction (figure 2(a)). A single thermal treatment at 660 °C is performed in order to remove residual stresses. The second one (sample B) is classified as a slightly unglassy state in which small crystals of $\beta$-quartz phase have formed (figure 2(b)) in the glassy phase. The structure of sample B is obtained after a two-step thermal treatment at plateau temperatures of $T_1 = 750\,^{\circ}\mathrm{C}$ and $T_2 = 900\,^{\circ}\mathrm{C}$. Both the size and the volume fraction of crystalline grains are evaluated by imaging the samples surface by AFM after a stay in fluorhydric acid (concentration ranging from 0.4 to 2%) for 30 s, which dissolves the amorphous phase faster than the crystalline one [14].

Fractures are then performed on the DCDC set-up [12, 15]: parallelepipedic ($4 \times 4 \times 40$ mm$^3$) samples (figure 3) are designed with a cylindrical hole (radius $a = 0.5$ mm) drilled in the centre and perpendicularly to the $4 \times 40$ mm$^2$ surface (figure 3). The hole axis defines the $z$-direction. The $x$-axis ($y$-axis) is parallel to the 40 mm (4 mm) side of the $4 \times 40$ mm$^2$ surfaces.

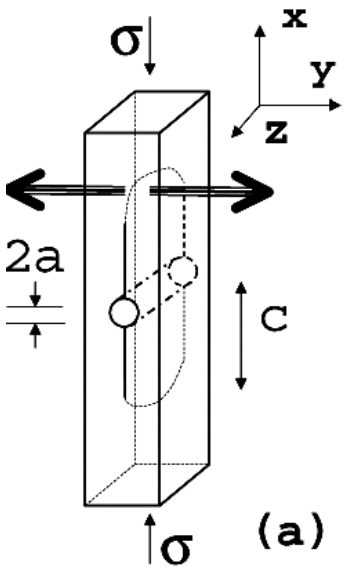


**Figure 3.** Sketch of the DCDC geometry.

In all cases, the $4 \times 40$ mm$^2$ surfaces are optically polished (the measured RMS roughness is around 0.25 nm for a $10 \times 10$ $\mu$m$^2$ scan-size). A compressive load is applied perpendicularly to the $4 \times 4$ mm$^2$ surfaces. The external stress $\sigma$ is gradually increased by the slow constant displacement (0.02 mm min$^{-1}$) of the jaws of the compressive machine (figure 1). Once the two cracks are initiated—symmetrically to the hole axis—the jaw displacement is stopped. The crack then propagates along the $x$-axis in the symmetry plane of the sample parallel to the $(x, z)$-plane. In this geometry, the stress intensity factor $K_I$ is given by [15]: $K_I = \sigma\sqrt{a}/(0.375c/a + 2)$, where $c$ is the crack length (figure 3).

The crack motion within the $(x, y)$ surface is monitored by our experimental system combining optical microscopy and AFM. Optical image processing gives the position of the crack tip (with a spatial resolution of 5 $\mu$m) and consequently the velocity for $v$ ranging from $10^{-6}$ to $10^{-9}$ m s$^{-1}$. Let us note that the measured 'instantaneous' velocity is actually averaged over a temporal window, the width of which is given by the time taken by the crack tip to advance a distance equal to the spatial resolution (typically 5000 s for a mean speed of $10^{-9}$ m s$^{-1}$). The crack tip neighbourhood can be probed by AFM measurements [16]—performed in a high-amplitude resonant mode ('tapping' mode)—at magnifications ranging from $75 \times 75$ nm$^2$ to $5 \times 5$ $\mu$m$^2$. The crack tip can be tracked at velocities ranging from $10^{-9}$ to $10^{-12}$ m s$^{-1}$. In the AFM case, the minimum width of the temporal window is reduced by two orders of magnitude thanks to the increased spatial resolution.

## 3. Crack tip velocity

In the very first moments, the crack propagates very quickly. In this regime, the crack velocity $v$ is independent of the chemical composition of the surrounding environment [9]. As the crack length $c$ increases, $K_I$ decreases, and $v$ decreases quickly. Under vacuum, the crack stops for $K_I$ smaller than a critical value $K_{Ic}$ referred to as the toughness of the material. But in a humid atmosphere, the corrosive action of water on glass allows for slow crack propagation at much lower values of stress [9]. When $K_I$ becomes smaller than the fracture toughness $K_{Ic}$

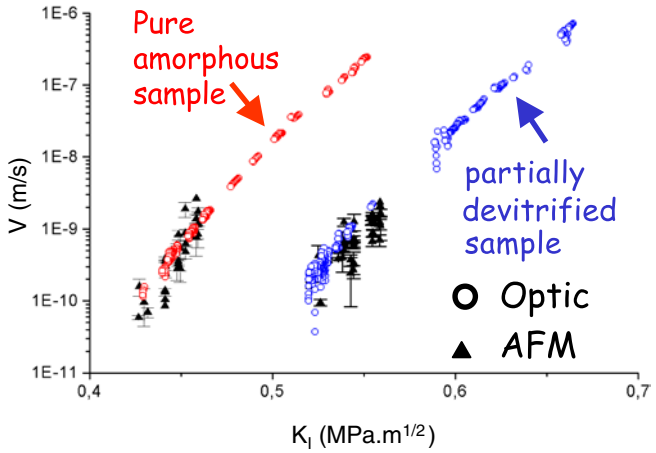


**Figure 4.** Variation of the crack tip velocity $v$ versus the stress intensity factor $K_I$. Open circles (black triangles) correspond to optical measurements (AFM measurements). The error bars correspond to the standard deviation on the velocity for a fixed value of the stress intensity factor $K_I$. For the lowest velocities $v$, the fluctuations are of the order of the average velocity.

(i.e. in the stress corrosion regime), the crack motion is slow enough to be monitored by our experimental system.

Figure 4 shows the variation of the velocity $v$ as a function of the stress intensity factor $K_I$ for both the amorphous and the partially devitrified specimens. The observed exponential behaviour is compatible with a stress-enhanced chemically activated process [9, 10].

The velocities measured for the partially devitrified sample (figure 4) are shifted towards positive $K_I$ when compared to the data relative to the amorphous sample. To understand this shift, we probe [14] the surface crack path at sub-micrometric scales (figure 5). In the partially devitrified specimen, the crystalline germs deflect the crack (figure 5(b)). As the crack tip keeps going through the amorphous phase, the stress-enhanced chemically activated process is identical in both samples (A and B) and consequently the slope of the semi-logarithmic curves $v(K_I)$ are the same in both the amorphous and the partially devitrified specimens. However, the deflections of the crack by the crystals induce local mode II and mode III components in the local stress intensity factor, which toughens the material [17]. Consequently, $K_{Ic}$ is larger in the devitrified sample, which shifts the $v(K_I)$ curve. A similar effect of the size of heterogeneities has been observed for the fatigue of metallic alloys [18].

The lowest velocities—only reachable thanks to the very high spatial resolution of AFM—shown in figure 4 exhibit important fluctuations, of the order of the average velocity, for *both* specimens [19]. Consequently, they cannot be related to the crystalline heterogeneities but are more likely inherent to the amorphous phase. The velocity fluctuations shown in figure 4 are of the order of $5 \times 10^{-11}$ m s$^{-1}$, i.e. of the same order of magnitude as the lowest measured averaged velocities; these fluctuations are the same in both specimens.

## 4. Evidence of nanometric cavities ahead of the crack tip

To understand the origin of the velocity fluctuation, we probed the neighbourhood of the crack tip at the nanometre scale in the amorphous specimen (figure 6). This clearly revealed the presence of cavities of typically 20 nm in length and 5 nm in width ahead of the crack tip (figure 6(a)) [20].

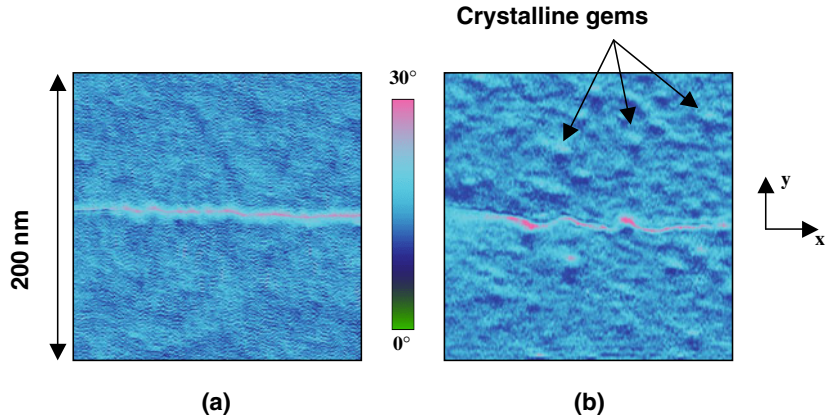


**Figure 5.** Crack path in (a) sample A (the amorphous specimen) and (b) sample B (the partially devitrified one). Frames are phase images sensitive to local mechanical properties, which allow us to distinguish the crystalline heterogeneities. In the partially devitrified sample, the crystals deflect the crack which propagates within the amorphous phase.

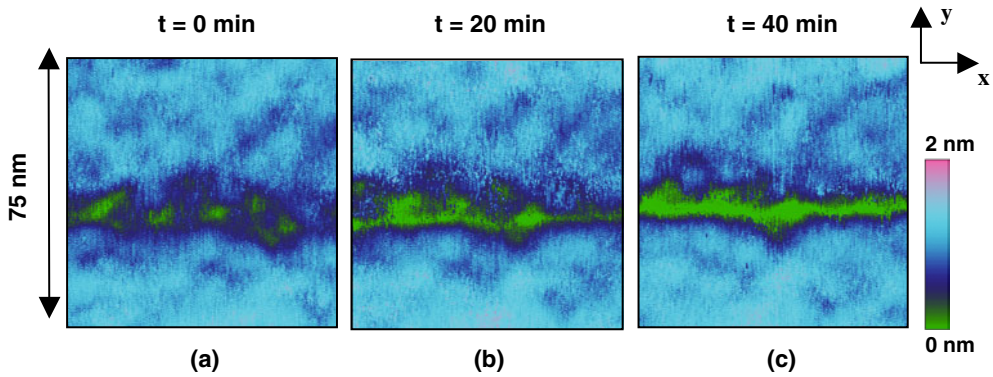


**Figure 6.** Sequence of successive topographic AFM frames showing the crack propagation at the surface of the specimen. The scan-size is 75 × 75 $nm^2$ and the heights range over 2 nm. The recording time for one frame is around 3 min and two successive frames are separated by 20 min. The crack front propagates from the left to the right ($x$-direction) with a mean velocity $v$ of around $10^{-11}$ m $s^{-1}$. (a) Evidence of nanometric damage cavities before the fracture advance, (b) growth of the cavities, (c) the crack is advancing via the coalescence of all the cavities.

These cavities grow with time (figure 6(b)) until they coalesce (figure 6(c)). At these nanometric scales, the crack front does not propagate regularly, but intermittently through the merging of the nanoscale cavities, which explains the large fluctuations observed for the lowest velocities (figure 4).

## 5. Nanometric cavities and nano-ductility

To ensure that the spots observed ahead of the crack tip are actually damage cavities which grow further and coalesce with the main crack leading to failure, we use the fracture surface topography analysis (FRASTA) technique first introduced to study damage in metallic alloys [21, 22]. These authors showed that, in a ductile scenario, each cavity initiation is accompanied by local irreversible plastic deformations *printed* in relief on the developing

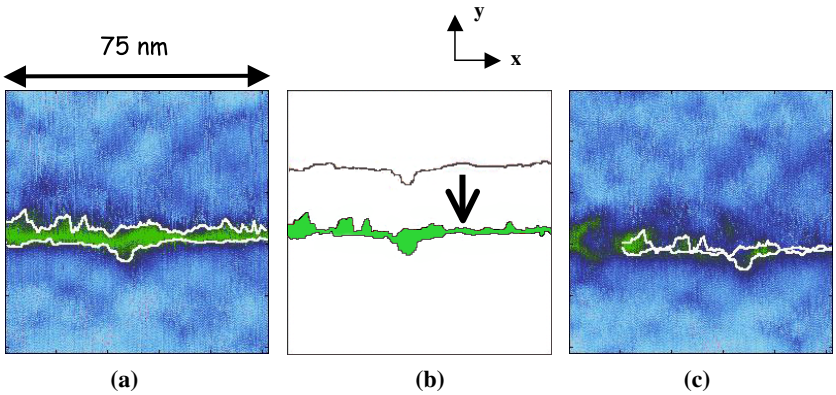


**Figure 7.** FRASTA. (a) Frame 4(c) (broken sample) is binarized and the contours of the crack are determined. (b) The lower line is first numerically raised over the upper one and then gradually displaced in the direction of decreasing $y$, as indicated by the arrow. Cavities are coloured in green. (c) Result of the method: superimposition of the obtained cavities on the image 6(b) recorded prior to complete failure.

fracture surfaces (the crack lines when the method is applied in two dimensions as in the present case) that should remain visible after the cavities have coalesced and the crack has crossed. The FRASTA method is designed to analyse the mismatch between the lower fracture surface (the lower crack line when the method is applied in two dimensions as in the present case) and the upper one (the upper crack line), mismatch due to the presence of cavities. For that purpose, the crack lines are first determined by binarizing the image of the sample after fracture (figure 7(a)), and the unbroken material is reconstituted virtually by placing numerically the lower line over the upper one (figure 7(b)). By translating the lower crack line gradually in the direction of decreasing $y$ (figure 7(b))—this displacement is what actually occurs during fracture—one can see the cavities appearing and growing in chronological order. The structure obtained for a given displacement, i.e. at a given time, is superimposed on images recorded prior to failure and is shown to correspond to cavities observed at this given time (figure 7(c)). This clearly indicates that the shape of the spots is determined well ahead of the crack tip, before the first spots can actually be observed, which provides a rather strong argument to relate these nanoscale spots to damage cavities.

This nanoscale ductility is also confirmed by the study of the displacement field around the crack tip (see also [23, 24] for related discussion); for a slit-like plane crack in an ideal Hookean continuum solid, all the components of the stress tensor are predicted to decrease as $r^{-1/2}$ with distance $r$ from the crack tip [25]. If the macroscopic stress–strain relation works at the nanometre scale, the depth $\delta$ (see the caption of figure 8 for a precise definition) should thus decrease as $r^{-1/2}$ in the vicinity of the crack tip during crack propagation. To be more precise, $\delta = Ar^{-1/2}\cos(\theta/2)$ for mode I fractures [26] where $A$ is a pre-factor depending only on the applied load and on the specimen geometry and $\theta$ is the angle between the direction of crack propagation and the $\vec{r}$ direction. Measurements of depth profiles have been performed on $1 \times 1\ \mu\text{m}^2$ AFM topographical frames (figure 8(a)) along the direction of crack propagation (figure 8(b)) and perpendicularly to it (figure 8(c)). For both profiles, $\delta$ departs from the linear elastic $r^{-1/2}$ scaling for $r$ smaller than a threshold $r_c$ highly dependent on $\theta$; for $\theta = 0°$, $r_c = 100$ nm while for $\theta = 90°$, $r_c = 20$ nm. These short range departures from the linear elastic behaviour may be related to the presence of cavities, although other phenomena could be responsible for this discrepancy (such as, for instance, the viscous effect, chemical effect etc).

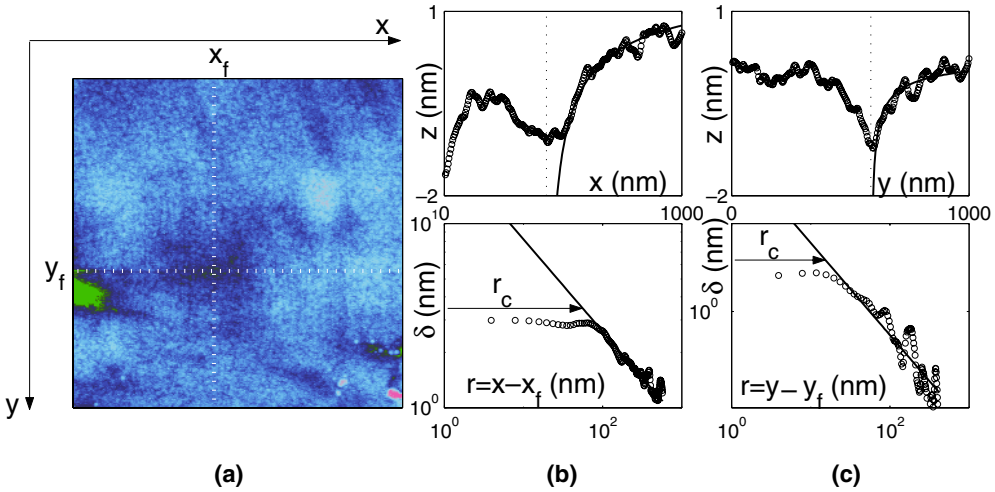


**Figure 8.** Measurements of the surface deformations and comparison with the predictions for an ideal Hookean material. The crack propagates from left to right ($x$ positive). (a) Typical AFM topographical frame of the vicinity of the crack tip. The scan-size is $1 \times 1\ \mu\text{m}^2$ and the heights range over 3 nm. The white vertical (horizontal) dotted line sets the $x$-coordinate $x_f$ ($y$-coordinate $y_f$) of the crack tip. (b) and (c) Upper plots: plot of the $z$ profile along (b) and perpendicular to (c) the direction of crack propagation. The open circles correspond to experimental data while the full line corresponds to the prediction $z = z_0 - Ar^{-1/2}$ (where $z_0$ and $A$ are fit parameters) given for an ideal Hookean solid. Lower plots: log–log plot of the depth $\delta = z_0 - z$ versus the distances $r = x - x_f$ (b) and $r = y - y_f$ (c) from the crack tip. For $r \leqslant r_c$, the $\delta$-profile departs from the predictions given by linear elastic theory.

However, the fact that the order of magnitude of the ratio $r_c(\theta = 0°)/r_c(\theta = 90°)$—much higher than the ratio of the cosine terms in the linear elastic expression of $\delta$—is close to the aspect ratio of the observed damage cavities, strongly suggests a correlation between damage and nonlinear elasticity.

## 6. Discussion

The same fracture experiments performed in amorphous silica specimens reveal similar damage cavities. This suggests that their existence does not depend on the precise chemical composition of the studied glass. The origin of the nucleation of cavities is more likely to be found in the amorphous structure, which contains inherent atomic density fluctuations at the nanometre scale. Such a scenario was indeed predicted by molecular dynamics simulation [27–30] that evidenced atomic density fluctuations in the structure of simulated amorphous silica; the Si and O atoms are shown to form silica tetrahedra connected together to build rings of different sizes ranging from three to nine tetrahedra. At larger length scales, ranging from 1.5 to 6 nm, the density of these rings is found to fluctuate, with high-density areas surrounded by low-density areas. Moreover, the molecular dynamics simulations of van Brutzel *et al* and Rountree *et al* [28–30] show that, at this length scale, cracks propagate by growth and coalescence of small cavities which appear in areas with a low density of rings, ahead of the crack tip. They behave as stress concentrators and grow under the stress imposed by the presence of the main crack to give birth to the cavities actually observed in the AFM frames.

The comparison of these theoretical results and the experimental evidence reported here strongly suggests that the advance of a crack in glass occurs by a ductile-like process—

at a temperature far below $T_g$—bound to nucleation, growth and coalescence of damage cavities. The nucleation of these damage cavities is very likely initiated within the low-density *nanometric* areas. The reason for the similarity between the two roughness regimes observed on post-mortem glass fracture surfaces [3, 4] can now be explained: the fracture advances through the nucleation, growth and coalescence of damage cavities in *both* brittle and ductile materials. The only difference lies in the length scales of the damage cavities; those related to 'brittle' materials are approximately three orders of magnitude smaller than those related to metallic alloys.

These observations strongly support the scenario proposed by Bouchaud *et al* [8]; the coalescence of the cavities is probably responsible for the observed roughness exponent of the $\zeta = 0.8$ regime observed at larger length scales (from $\xi_c$ to 100 nm). The order of magnitude of $\xi_c$ is indeed in good agreement with our present observations, where cavities at coalescence are a few tens of nanometres wide. On the other hand, the $\zeta = 0.5$ regime observed for smaller length scales is probably related to an irregular start–stop motion characteristic of the non-equilibrium dynamic critical-point at which the crack starts to advance. This may generate diffusely damped crack-front corrugations, leading to a steady state roughening of fracture surfaces. This effect is predicted to occur even though the macroscopic velocity of the crack front is small, provided that the instantaneous velocity during an 'avalanche' in a strongly heterogeneous medium may reach much higher values. This may have been at the origin of the important fluctuations in crack velocities reported in the present paper.

Here, let us note that AFM observations are performed on the sample surface, where the mechanical state is different from that of the bulk. Hence, the observed sizes and growth rates of cavities at the surface may well differ from those in the bulk. New experiments using the FRASTA method in three dimensions applied to the post-mortem study of the fracture surfaces are currently being performed, in order to have access to the three-dimensional structure of bulk damage and its evolution. Through this new set of experiments, we should be able to correlate also the damage structure to the fracture surface morphology.

The topographic study of post-mortem surfaces will also be a good experimental test of the validity of the work of Bouchaud *et al* [8]. This scenario suggests that a small length scale exponent $\zeta = 0.5$ is due to the existence of diffusively broadened crack-front waves in localized depinning events. Other important predictions are that the roughness amplitude should be strongly anisotropic and this effect should be very pronounced at low crack growth velocities. That model also predicts that the physics of the formation and coalescence of the cavities is responsible for the observed roughness exponent of $\zeta = 0.8$. Observations of the roughness of growing cavities before coalescence in an aluminium alloy [7] have already proved that this scenario is realistic. It will, of course, be crucial—even if much more experimentally difficult due to a much lower $\xi_c$ value—to check these hypotheses in the case of nano-ductile materials.

Moreover, the structure of the damage, which influences macroscopic mechanical properties such as fracture toughness and lifetime, must then be linked to the glass composition and nanostructure [28, 31–33]. Complementary analyses addressing the question of the chemical bonds on the fracture surface should also be performed.

## 7. Conclusion

Quasi-static fracture in glassy materials has been studied *in real-time* at sub-micrometric length scales in a wide velocity range. The crack velocities are measured as a function of the stress intensity factor in both amorphous materials and a partially devitrified one. Important fluctuations are reported for the lowest velocities. They are conjectured to be related to the presence—inside the glassy phase—of nanoscale damage cavities observed in real-time ahead

of the crack tip. The influence of these damage cavities on mechanical properties outside the purely elastic zone in the vicinity of the crack tip have been presented. These results confirm the scenario proposed by Bouchaud *et al* [8] to explain the origin of the two self-affine regimes observed on fracture surfaces. The implications of such a ductile fracture mode in glass on the morphology of the fracture surfaces have been discussed. However, it should be noted that our investigations are performed on the sample surface while the fracture surface morphology is related to the fracture of bulk. Consequently, it would be interesting to investigate the 3D distribution of damage cavities. Work in this direction is currently in progress.

Finally, the fact that glass, at temperatures far below the glass transition temperature $T_g$, joins the class of damageable materials should have important consequences for its mechanical properties. In applications, the design of structures using glass might be modified to take this behaviour into account, especially for slow crack propagation processes.

The similarity between the damage modes of materials as different as glass and metallic alloys is an important clue to aid our understanding of the origin of some puzzling universal behaviour, hence shedding new light on the basic physical mechanisms of fracture.

## References


[1] Pineau A, François D and Zaoui A 1995 *Comportement Mécanique des Matériaux* (Paris: Hermès)
[2] Mandelbrot B B, Passoja D E and Paullay A J 1984 *Nature* **308** 721
[3] Bouchaud E 1997 *J. Phys.: Condens. Matter* **9** 4319 and references therein
[4] Daguier P *et al* 1997 *Phys. Rev. Lett.* **78** 1062
[5] Poor C Y, Sayles R S and Jones T A 1992 *J. Phys. D: Appl. Phys.* **25** 1269
[6] Bouchaud E and Paun F 1999 *Comput. Sci. Eng.* **September/October** 32–8
[7] Paun F and Bouchaud E 2003 *Morphology of Damage Cavities* in preparation
[8] Bouchaud E *et al* 2002 *J. Mech. Phys. Solids* **50** 1703
[9] Wiederhorn S M 1967 *J. Am. Ceram. Soc.* **50** 407
[10] Wiederhorn S M and Bolz L H 1970 *J. Am. Ceram. Soc.* **53** 543
[11] Michalske T A, Smith W L and Bunker B C 1991 *J. Am. Ceram. Soc.* **74** 1993
[12] Janssen C 1974 *Proc. 10th Int. Congr. on Glass* p 3453
[13] Marlière C, Despetis F and Phalippou J 2003 *J. Non-Cryst. Solids* **316** 21
[14] Dickelé A 2002 Etude structurale et mécanique d'un matériau vitreux soumis à la fracturation *Master Thesis* Université Montpellier 2
[15] He M Y, Turner M R and Evans A G 1995 *Acta Mater.* **43** 3453
[16] Marlière C *et al* 2001 *J. Non-Cryst. Solids* **285** 148
[17] Faber K T and Evans A G 1983 *Acta Metall.* **31** 565
[18] Ducourthial E, Bouchaud E and Chaboche J-L 2000 *Comput. Mater. Sci.* **19** 229
[19] Célarié F, Prades S, Bonamy D, Ferrero L, Bouchaud E, Guillot C and Marlière C 2003 *Appl. Surf. Sci.* at press
[20] Célarié F, Prades S, Bonamy D, Ferrero L, Bouchaud E, Guillot C and Marlière C 2003 *Phys. Rev. Lett.* **90** 075504
[21] Kobayashi T and Shockey D A 1987 *Metall. Trans.* A **18** 1941
[22] Miyamoto H, Kikuchi M and Kawazoe T 1990 *Int. J. Fract.* **42** 389
[23] Guilloteau E, Charrue H and Creuzet F 1996 *Europhys. Lett.* **34** 549
[24] Hénaux S and Creuzet F 2000 *J. Am. Ceram. Soc.* **83** 415
[25] Irwin G R 1957 *J. Appl. Mech.* **24** 361
[26] Lawn B R 1993 *Fracture of Brittle Solids* 2nd edn (Cambridge: Cambridge University Press)
[27] Nakano A, Kalia R K and Vashishta P 1995 *Phys. Rev. Lett.* **75** 3138
Vashishta P, Kalia R K and Nakano A 1999 *Comput. Sci. Eng.* **September/October** 56–65
Campbell T *et al* 1999 *Phys. Rev. Lett.* **82** 4018
[28] Van Brutzel L 1997 *PhD Thesis*
[29] Van Brutzel L *et al* 2002 *Mater. Res. Soc. Symp. Proc.* **703** V3.9.1
[30] Rountree L *et al* 2002 *Annu. Rev. Mater. Res.* **32** 377
[31] Falk M L 1999 *Phys. Rev.* B **60** 7062
Falk M L and Langer J S 2000 *MRS Bull.* **25** 40
[32] Benoit M *et al* 2000 *Eur. Phys. J.* B **13** 631
[33] Jund P, Kob W and Jullien R 2001 *Phys. Rev.* B **64** 134303